Construction of the one-point PDF of the local aperture mass in weak lensing maps

F. Bernardeau and P. Valageas

Service de Physique Théorique, CEA de Saclay, 91191 Gif-sur-Yvette, France

Abstract. We present a general method for the reconstruction of the one-point Probability Distribution Function of the local aperture mass in weak lensing maps. Exact results, that neglect the lens-lens coupling and departure from the Born approximation, are derived for both the quasilinear regime at leading order and the strongly nonlinear regime assuming the tree hierarchical model is valid. We describe in details the projection effects on the properties of the PDF and the associated generating functions. In particular, we show how the generic features which are common to both the quasilinear and nonlinear regimes lead to two exponential tails for $P(M_{\rm ap})$. We briefly investigate the dependence of the PDF with cosmology and with the shape of the angular filter. Our predictions are seen to agree reasonably well with the results of numerical simulations and should be able to serve as foundations for alternative methods to measure the cosmological parameters that take advantage of the full shape of the PDF.

Key words: cosmology: theory – cosmology: gravitational lensing – cosmology: large-scale structure of Universe

1. Introduction

Recent reports of cosmic shear detection (van Waerbeke et al. 2000a; Bacon et al. 2000; Wittman et al. 2000; Kaiser et al. 2000) have underlined the interest that such observations can have for exploring the large-scale structures of the Universe. Previous papers have stressed that not only it could be possible to measure the projected power spectrum (Blandford et al. 1991; Miralda-Escudé 1991; Kaiser 1992) of the matter field, but also that non-linear effects could be significant and betray the value of the density parameter of the Universe. More specifically, Bernardeau et al. (1997) have shown that the skewness, third order moment of the local convergence field, when properly expressed in terms of the second moment can be a probe of the density parameter independently of the amplitude of the density fluctuations. This result can be extended to higher order moments, to the nonlinear regime (Jain & Seljak 1997; Hui 1999; Munshi & Coles 2000; Munshi & Jain 1999b) and the whole shape of the one-point PDF (Valageas 2000a,b; Munshi & Jain 1999a,b).

In case of weak lensing surveys it appears however that it is more convenient to consider the so called aperture mass statistics that corresponds to filtered convergence fields with a compensated filter, that is with a filter of zero spatial average (Kaiser et al. 1994; Schneider 1996). Indeed, it is possible to relate the local aperture mass to the observed shear field only, whereas, in contrast, convergence maps require the resolution of a non-local inversion problem and are only obtained to a mass sheet degeneracy. The aperture mass statistics have proved valuable in particular for cosmic variance related issues (Schneider et al. 1998). Thus, in this article we present a method to compute the one-point PDF of the aperture mass, both for the quasilinear and strongly non-linear regimes. In the case of the quasilinear regime we can use rigorous perturbative methods while in the highly non-linear regime we have to use a specific hierarchical tree model (which has been seen to agree reasonably well with numerical simulations). Although the details of the calculations are specific to each case we point out the general pattern common to both regimes which is brought about by the projection effects. In particular, our methods are quite general and actually apply to any filters, though we are restricted to axisymmetric filters for the quasi-linear regime. Our results for the non-linear regime, where there is not such a restriction, can also be extended to multivariate statistics ($p-$point PDFs).

In Sect. 2 we recall the definitions of the local convergence and aperture mass and how they are related to the cosmic 3D density fluctuations. In particular we present the shape of the compensated filters that we use for the explicit computations we present in the following. In Sect. 3 we describe the relationship between the PDF and the cumulant generating function of the 3D density field and we show how this extends to the projected density. The details of the calculations are presented in Sect. 4, for the quasilinear theory, and in Sect. 5 for the nonlinear theory. Numerical results are presented in Sect. 6.

2. The convergence and aperture mass fields

In weak lensing observations, background galaxy deformations can be used to reconstruct the local gravitational convergence field. We recall here how the local convergence is related to the line-of-sight cosmic density fluctuations. As a photon travels from a distant source towards the observer its trajectory is per-

turbed by density fluctuations close to the line-of-sight. This leads to an apparent displacement of the source and to a distortion of the image. In particular, the convergence κ magnifies (or de-magnifies) the source as the cross section of the beam is decreased (or increased). One can show (Kaiser 1998) that the convergence along a given line-of-sight is,

$$\kappa = \int_0^{\mathcal{R}_s} d\mathcal{R} \ \hat{w}(\mathcal{R}, \mathcal{R}_s) \ \delta(\mathcal{R}) \tag{1}$$

when lens-lens couplings and departure from the Born approximation are neglected (e.g., Bernardeau et al. 1997). This equation states that the local convergence is obtained by an integral over the line-of-sight of the local density contrast. The integration variable is the radial distance, $\mathcal{R}$, (and $\mathcal{R}_s$ corresponds to the distance of the source) such that

$$d\mathcal{R} = \frac{c \, dz/H_0}{\sqrt{\Omega_\Lambda + (1 - \Omega_m - \Omega_\Lambda)(1 + z)^2 + \Omega_m(1 + z)^3}} \tag{2}$$

while the angular distance $\mathcal{D}$ is defined by,

$$\mathcal{D}(z) = \frac{c/H_0}{\sqrt{1 - \Omega_m - \Omega_\Lambda}} \sinh\left(\sqrt{1 - \Omega_m - \Omega_\Lambda} \ \frac{H_0 \mathcal{R}}{c}\right) \tag{3}$$

Then, the weight $\hat{w}(\mathcal{R}, \mathcal{R}_s)$ used in (1) is given by:

$$\hat{w}(\mathcal{R}, \mathcal{R}_s) = \frac{3\Omega_m}{2} \frac{H_0^2}{c^2} \frac{\mathcal{D}(\mathcal{R})\mathcal{D}(\mathcal{R}_s - \mathcal{R})}{\mathcal{D}(\mathcal{R}_s)} (1 + z) \tag{4}$$

where z corresponds to the radial distance $\mathcal{R}$. Thus the convergence κ can be expressed in a very simple fashion as a function of the density field. We can note from (1) that there is a minimum value $\kappa_{\min}(z_s)$ for the convergence of a source located at redshift z_s, which corresponds to an "empty" beam between the source and the observer ($\delta = -1$ everywhere along the line-of-sight):

$$\kappa_{\min} = -\int_0^{\mathcal{R}_s} d\mathcal{R} \ \hat{w}(\mathcal{R}, \mathcal{R}_s) \tag{5}$$

In practice, rather than the convergence κ it can be more convenient (Schneider 1996) to consider the aperture mass M_{ap}. It corresponds to a geometrical average of the local convergence with a window of vanishing average,

$$M_{ap} = \int d^2\vartheta' \ U(\vartheta') \ \kappa(\vartheta' - \vartheta) \tag{6}$$

where $\kappa(\vartheta)$ is the local convergence at the angular position ϑ and the window function U is such that

$$\int d^2\vartheta \ U(\vartheta) = 0. \tag{7}$$

In this case, M_{ap} has the interesting property that it can be expressed as a function of the tangential component γ_t of the shear (Kaiser et al. 1994; Schneider 1996) so that it is not in principle necessary to build local shear maps to get local aperture mass maps. More precisely we can write,

$$M_{ap}(\vartheta) = \int d^2\vartheta' \ Q(\vartheta') \ \gamma_t(\vartheta - \vartheta') \tag{8}$$

with

$$Q(\vartheta) = -U(\vartheta) + \frac{2}{\vartheta^2} \int d\vartheta' \ \vartheta' \ U(\vartheta'). \tag{9}$$

Nonetheless considering such a class of filters is interesting because convergence maps are always reconstructed to a mass sheet degeneracy only. Therefore, to some extent, any statistical quantities that can be measured in convergence mass maps correspond to smoothed quantities with compensated filters. In the following, for convenience rather than due to intrinsic limitation of the method, we consider filters that are defined on a compact support.

2.1. Choice of filter

It is convenient to write the filter function in terms of reduce variable, ϑ/θ where θ is the filter scale,

$$U(\vartheta) = \frac{u(\vartheta/\theta)}{\theta^2} \tag{10}$$

so that the evolution with θ of the properties of M_{ap} only depends on the behavior of the density field seen on different scales (while the shape and the normalization of the angular filter $U(\vartheta)$ remains constant). In the following we shall use two different filters, which satisfy (10). One, which we note u_S, has been explicitly proposed by Schneider (1996),

$$u_S(x) = \frac{9}{\pi} (1 - x^2) \left(\frac{1}{3} - x^2\right) \quad \text{for } x < 1 \tag{11}$$

and $u_S(x) = 0$ otherwise. The Fourier form of this filter corresponds to,

$$W_S(l) = 2\pi \int_0^1 dx \ x \ u_S(x) \ J_0(lx) = \frac{24 \, J_4(l)}{l^2}. \tag{12}$$

The other, which we note u_{BV}, corresponds to a simpler compensated filter that can be built from two concentric discs. It is built from the difference of the average convergence in a disc $1/2$ and the average convergence in a disc unity:

$$u_{BV}(x) = \frac{4H(2x)}{\pi} - \frac{H(x)}{\pi} \tag{13}$$

where $H(x)$ is the characteristic function of a disc unity. In Fourier space it is simply related to the Fourier transform of a disc of radius unity,

$$W_1(l) = \frac{2 \, J_1(l)}{l}, \tag{14}$$

and reads,

$$W_{BV}(l) = W_1(l/2) - W_1(l) = \frac{4 \, J_1(l/2)}{l} - \frac{2 \, J_1(l)}{l}. \tag{15}$$

The ratio of the 2 radii has been chosen so that the 2 filters are close enough, as shown in Fig. 1. Note that the normalizations are somewhat arbitrarily. In the plot they have been chosen to give the same amplitude for the aperture mass fluctuations in case of a power law spectrum with index $n = -1.5$. This is
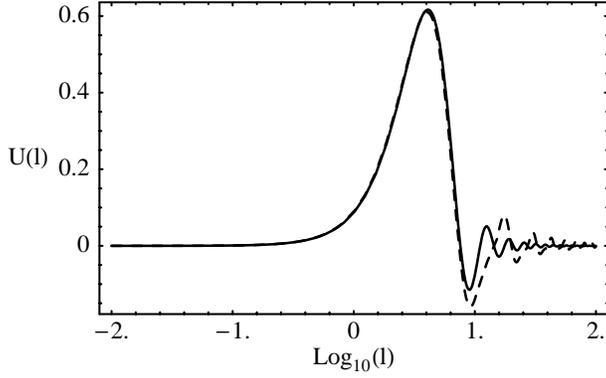
Fig. 1. Shape of the filter functions we use in Fourier space. The solid line corresponds to the shape proposed by Schneider, Eq. (12), multiplied by 1.459 and the dashed line corresponds to the compensated filter we introduce in this paper, Eq. (15).

obtained by multiplying the expression (12) by 1.459. Fig. 1 shows actually that the two filters are very close to each other. In particular they have their maximum at the same k scale, and except for the large k oscillations they exhibit a similar behavior. In the following we will take the freedom to use either one or the other for convenience.

3. One-point PDF construction

In this section we succinctly review the theory for the construction of the one-point PDF statistical quantities. In particular we recall the mathematical relationship between the one-point PDF and the moment and cumulant generating functions.

3.1. General formalism

In general one can define $\chi(\lambda)$ as the generating function of the cumulants of a given local random variable δ,

$$\chi(\lambda) = \sum_{p=1}^{\infty} \langle \delta^p \rangle_c \frac{\lambda^p}{p!}. \tag{16}$$

It is given through a Laplace transform of the one-point PDF of the local density contrast δ,

$$e^{\chi(\lambda)} = \int_{-1}^{\infty} \mathrm{d}\delta \, e^{\lambda \delta} \, P(\delta). \tag{17}$$

For hierarchical models, that is when $\langle \delta^p \rangle_c \sim \langle \delta^2 \rangle^{p-1}$ it is convenient to define $\varphi(y)$ as

$$\varphi(y) = -\sum_p \frac{\langle \delta^p \rangle_c}{\langle \delta^2 \rangle^{p-1}} \frac{(-y)^p}{p!} = -\langle \delta^2 \rangle \, \chi(-y/\langle \delta^2 \rangle). \tag{18}$$

Then the one-point PDF of δ is then given by the inverse Laplace transform (see Balian & Schaeffer 1989),

$$P(\delta)\mathrm{d}\delta = \mathrm{d}\delta \int \frac{\mathrm{d}y}{2\pi\mathrm{i}\sigma^2} \exp\left[-\frac{\varphi(y)}{\sigma^2} + \frac{y\delta}{\sigma^2}\right], \tag{19}$$

of the moment generating function. Here $\sigma = \langle \delta^2 \rangle^{1/2}$ is the r.m.s. density fluctuation.

3.2. The projection effects

The relation (1) states that the local convergence can be viewed as the superposition of independent layers of cosmic matter field. The direct calculation of the one-point PDF of such a sum would involve an infinite number of convolution products which makes it intractable. It is more convenient to consider the cumulant generating functions which simply add when different layers are superposed (because Laplace transforms change convolutions into ordinary products).

The projections effects for statistical properties of the local convergence have already been considered in previous papers. It has been shown in particular how the moments of the projected density can be related to the ones of the 3D field in both hierarchical models corresponding to the non-linear regime (Tóth et al. 1989) and in the quasilinear regime (Bernardeau 1995).

More recently it has been shown (Valageas 2000a,b; Munshi & Jain 1999a) that these results could be extended to the full PDF of the projected density. In particular the cumulant generating function of the projected density can be obtained by a simple line-of-sight average of the 3D cumulant generating function.

It is convenient to define the normalized projected density contrast $\delta_{\mathrm{proj.}}$ by:

$$\delta_{\mathrm{proj.}} = \frac{\kappa}{|\kappa_{\min}|} = \int \mathrm{d}\mathcal{R} \, F(\mathcal{R}) \, \delta(\mathcal{R}), \tag{20}$$

where $F(\mathcal{R})$ is the selection function for the projection effects as a function of the radial distance $\mathcal{R}$:

$$F(\mathcal{R}) = \frac{\hat{w}(\mathcal{R}, \mathcal{R}_s)}{|\kappa_{\min}|}. \tag{21}$$

When filtering effects are included we have,

$$\delta_{\mathrm{proj.},\theta} = \int \mathrm{d}^2\vartheta' \, w_\theta(\vartheta') \, \delta_{\mathrm{proj.}}(\vartheta' - \boldsymbol{\vartheta}) \tag{22}$$

where w_θ is a given window function at scale θ. A particular case is provided by the normalized aperture mass $\hat{M}_{\mathrm{ap}}$,

$$\hat{M}_{\mathrm{ap}} = \frac{M_{\mathrm{ap}}}{|\kappa_{\min}|} = \int \mathrm{d}^2\vartheta' \, U(\vartheta') \, \delta_{\mathrm{proj.}}(\boldsymbol{\vartheta}' - \boldsymbol{\vartheta}). \tag{23}$$

The cumulants of the projected density can be related to those of the 3D density fields. Formally they correspond to the ones of the field when it is filtered by a conical shape window. Thus, from (20) we obtain:

$$\langle \delta_{\mathrm{proj.}}(\boldsymbol{\vartheta}_1) \ldots \delta_{\mathrm{proj.}}(\boldsymbol{\vartheta}_p) \rangle_c = \int_0^{\mathcal{R}_s} \prod_{i=1}^{p} \mathrm{d}\mathcal{R}_i \, F(\mathcal{R}_i)$$
$$\times \langle \delta(\mathcal{R}_1, \mathcal{D}_1\boldsymbol{\vartheta}_1) \ldots \delta(\mathcal{R}_p, \mathcal{D}_p\boldsymbol{\vartheta}_p) \rangle_c. \tag{24}$$

The computation of such quantities can be made in the small angle approximation. Such approximation is valid when the transverse distances $\mathcal{D}|\boldsymbol{\vartheta}_i - \boldsymbol{\vartheta}|$ are much smaller than the radial distances $\mathcal{R}$. In this case the integral (24) is dominated by configurations where $\mathcal{R}_i - \mathcal{R}_j \sim \mathcal{D}_i|\boldsymbol{\vartheta}_i - \boldsymbol{\vartheta}_j| \sim \mathcal{D}_j|\boldsymbol{\vartheta}_i - \boldsymbol{\vartheta}_j|$. It permits to make the change of variables $\mathcal{R}_i \to r_i$ with $\mathcal{R}_i = \mathcal{R}_1 + r_i\mathcal{D}_1$. Then, since the correlation length (beyond which the many-body correlation functions are negligible) is much smaller than

the Hubble scale $c/H(z)$ (where $H(z)$ is the Hubble constant at redshift z) the integral over r_i converges over a small distance of the order of $|\boldsymbol{\vartheta}_i - \boldsymbol{\vartheta}_1|$ and the expression (24) can be simplified in,

$$\langle \delta_{\text{proj.}}(\boldsymbol{\vartheta}_1) \dots \delta_{\text{proj.}}(\boldsymbol{\vartheta}_p) \rangle_c = \int_0^{\mathcal{R}_s} \mathcal{D}_1^{p-1} d\mathcal{R}_1 \ F_1^p$$
$$\times \int_{-\infty}^{\infty} \prod_{i=2}^{p} dr_i \ \langle \delta(\mathcal{R}_1, \mathcal{D}_1 \boldsymbol{\vartheta}_1) \dots \delta(\mathcal{R}_1 + r_i \mathcal{D}_1, \mathcal{D}_1 \boldsymbol{\vartheta}_p) \rangle_c. (25)$$

Taking filtering effects into account leads to,

$$\langle \delta_{\text{proj.},\theta}^p \rangle_c = \int_0^{\mathcal{R}_s} \mathcal{D}_1^{p-1} d\mathcal{R}_1 \ F_1^p \int \prod_{i=1}^{p} d^2\vartheta_i \, w_\theta(\vartheta_i)$$
$$\times \int_{-\infty}^{\infty} \prod_{i=2}^{p} dr_i \ \langle \delta(\mathcal{R}_1, \mathcal{D}_1 \boldsymbol{\vartheta}_1) \dots \delta(\mathcal{R}_1 + r_i \mathcal{D}_1, \mathcal{D}_1 \boldsymbol{\vartheta}_p) \rangle_c. (26)$$

Thus the projection effects reduce to

$$\langle \delta_{\text{proj.},\theta}^p \rangle_c = \int d\mathcal{R} \ F^p(\mathcal{R}) \langle \delta_{\mathcal{D}\theta, \text{cyl.}}^p \rangle_c \ L^{p-1}, \tag{27}$$

where $\delta_{\mathcal{D}\theta, \text{cyl.}}^p$ is the filtered 3D density with a cylindrical filter of transverse size $\mathcal{D}\theta$ and depth L (which goes to infinity in (25)).

In particular this result gives the expression of the variance of the filtered projected density contrast,

$$\langle \delta_{\text{proj.},\theta}^2 \rangle = \int_0^{\mathcal{R}_s} d\mathcal{R} \ F^2(\mathcal{R}) \langle \delta_{\mathcal{D}\theta, \text{cyl.}}^2 \rangle_c \ L \tag{28}$$

This expression can be re-expressed in terms of the power spectrum $P(k)$ (nonlinear power spectrum), defined in this paper with

$$\langle \delta(\mathbf{x}_1) \delta(\mathbf{x}_2) \rangle = \int \frac{d^3\mathbf{k}}{(2\pi)^3} P(k) \, e^{i\mathbf{k}(\mathbf{x}_1 - \mathbf{x}_2)}. \tag{29}$$

Then

$$\langle \delta_{\mathcal{D}\theta, \text{cyl.}}^2 \rangle_c = \int_0^{\infty} \frac{dk_\parallel}{2\pi} \int \frac{d^2\mathbf{k}_\perp}{(2\pi)^2} P(k)$$
$$\times \left[\frac{2 \sin(k_\parallel L)}{k_\parallel L} \right]^2 W^2(\mathcal{D}\theta k_\perp) \tag{30}$$

where $\mathbf{k}_\perp$ is the component of $\mathbf{k}$ orthogonal to the radial direction and $k_\parallel$ is the component along the line-of-sight. In the previous integral, $k_\parallel \sim 1/L$ and $k_\perp \sim 1/(\mathcal{D}\theta)$, so that when L is large $k_\parallel$ is negligible compared to $k_\perp$ which leads to,

$$\langle \delta_{\mathcal{D}\theta, \text{cyl.}}^2 \rangle = \frac{1}{L} \int \frac{d^2\mathbf{k}_\perp}{(2\pi)^2} P(k_\perp) W^2(\mathcal{D}\theta \mathbf{k}_\perp) \tag{31}$$

where W is the Fourier shape of the 2D window function. This relation holds for the filtered projected density contrast as well as the aperture mass, for which W in (31) is to be replaced by W_S or W_{BV}.

The formal expression for the higher order moments can be simplified by taking advantage of the so-called scaling laws for the correlation functions. It is in particular natural to assume that,

$$\langle \delta^p \rangle_c \propto \langle \delta^2 \rangle^{p-1} \tag{32}$$

with a coefficient of proportionality, S_p, that depends on both the power spectrum and filter shapes, but not on the power spectrum normalization. For power law spectrum it implies in particular that these coefficients do not depend on the filtering scale. In the coming sections we present in more details the origin of this scaling relation. It allows to define

$$\varphi(y) \equiv -\sum_p S_p \frac{(-y)^p}{p!} = -\langle \delta^2 \rangle \, \chi(-y/\langle \delta^2 \rangle). \tag{33}$$

The Eq. (27) then relates the cumulant generating function $\varphi(y)$ for the projected density to the one corresponding to cylindrical filtering effects,

$$\varphi_{\text{proj.}}(y) = \int \frac{d\mathcal{R}}{\psi_\theta(\mathcal{R})} \varphi_{\text{cyl.}}[y \, F(\mathcal{R}) \psi_\theta(\mathcal{R})] \tag{34}$$

with

$$\psi_\theta(\mathcal{R}) = \frac{\langle \delta_{\mathcal{D}\theta, \text{cyl.}}^2 \rangle}{\langle \delta_{\text{proj.},\theta}^2 \rangle} L \tag{35}$$

which can be rewritten in terms of the matter fluctuation power spectrum,

$$\psi_\theta(\mathcal{R}) = \frac{\int d^2\mathbf{k} \, P(k, z) \, W^2(k \, \mathcal{D}\theta)}{\int d\mathcal{R}' \, F^2(\mathcal{R}') \int d^2\mathbf{k} \, P(k, z') \, W^2(k \, \mathcal{D}'\theta)}. \tag{36}$$

In this expression we have explicitly written the redshift dependence of the power spectrum. In case of a power law spectrum,

$$P(k, z) = P_0(z) \left(\frac{k}{k_0} \right)^n \tag{37}$$

it takes a much simpler form given by,

$$\psi_\theta(\mathcal{R}) = \frac{P_0(z) \, \mathcal{D}^{-n-2}}{\int d\mathcal{R}' \, F^2(\mathcal{R}') \, P_0(z') \, \mathcal{D}'^{-n-2}}. \tag{38}$$

The result (34) is the cornerstone of the calculations we present. It allows to relate the cumulant generating function of projected quantities to the ones computed in much simpler geometries.

The difficulty then resides in the computation of $\varphi_{\text{cyl.}}$ in the regimes we are interested in. Two limit cases are actually accessible to exact calculations. First, one is the quasilinear regime where one can take advantage of the special properties of the perturbative expansion in Lagrangian space to build the cumulant generating function in Eulerian space. These kinds of properties had been used previously for 3D or 2D top-hat filters only. We show here how this method can be extended to the filter (15). Second, in the strongly nonlinear regime one can also do exact numerical calculations when one is assuming the high order correlation functions to follow a tree model. The derivations corresponding to these regimes are presented in the next two sections.

4. The quasi-linear regime

The reason rigorous calculations can be carried on in this regime is that the cumulant generating function for a cylindrical shape is exactly the one corresponding to the 2D dynamics (Bernardeau 1995). In other words, in this case

$$\varphi_{\text{cyl.}}^{\text{quasilinear}}(y) = \varphi_{2D}^{\text{quasilinear}}(y) \tag{39}$$

at leading order. In this regime the problem then reduces to the computation of cumulant generating functions for compensated filters for the 2D dynamics. The latter calculation is presented in the following paragraphs. This is a long and technical calculation that leads to the formulae (85-87).

The calculations we present follow what has been done for the top-hat window filters, with the complication introduced by the use of two such filters instead of one to build the compensated filter.

4.1. 2D statistics in Lagrangian space

The generating function for the compensated filter (13) can be built from the generating function of the joint density PDF for two concentric cells of different radius. This quantity will be obtained in Eulerian space from the one in Lagrangian space through a Lagrangian-Eulerian mapping. More precisely we consider the joint PDF of two reduced volumes defined as the comoving volume $V_c(t)$ occupied by some matter expressed in units of the volume V it occupied initially,

$$v = \frac{V_c(t)}{V}. \tag{40}$$

The Eulerian overdensity of this matter region will then be given by the inverse of v,

$$\rho = 1/v. \tag{41}$$

The calculation will be made in two steps. First we present the derivation of the cumulant generating function in Lagrangian space, then the mapping from Lagrangian to Eulerian space.

In a Lagrangian description v corresponds to the Jacobian of the transform from the initial coordinates $\mathbf{q}$ in Lagrangian space to the ones in real space $\mathbf{x}$,

$$v = J(\mathbf{q}) = \left| \frac{\partial \mathbf{x}}{\partial \mathbf{q}} \right|. \tag{42}$$

The construction of the volume PDF is then based on the geometrical properties of the Jacobian perturbative expansion. Its expansion with respect to the initial density fluctuations (in the rest of this subsection we consider 2D dynamics) reads

$$J(\mathbf{q}) = 1 + J^{(1)}(\mathbf{q}) + \dots \tag{43}$$

Each term of this expansion can be written in terms of the initial Fourier modes of the linear density field,

$$J^{(p)} = \int \frac{d^2\mathbf{k}_1}{2\pi} \dots \frac{d^2\mathbf{k}_p}{2\pi} D_+^p(t) \, \delta(\mathbf{k}_1) \dots \delta(\mathbf{k}_p) \times$$
$$\exp[i(\mathbf{k}_1 + \dots + \mathbf{k}_p)\mathbf{q}] \, J_p(\mathbf{k}_1, \dots, \mathbf{k}_p). \tag{44}$$

where $D_+(t)$ describes the time dependence of the linear growing mode. The central issue is the way the geometrical kernel $J_p(\mathbf{k}_1, \dots, \mathbf{k}_p)$ behaves when geometrical effects are taken into account. At leading order in perturbation theory (that is when only "tree order" terms are taken into account) that amounts to compute terms of the form

$$\int d\alpha_1 \dots d\alpha_p \, J_p(\mathbf{k}_1, \dots, \mathbf{k}_p) \, W|\mathbf{k}_1 + \dots + \mathbf{k}_p|. \tag{45}$$

where α_i is the angle of the ith wave vector. There exists a central property, valid for top-hat filters only, which states that (Bernardeau 1995),

$$\int d\alpha_1 \dots d\alpha_p \, J_p(\mathbf{k}_1, \dots, \mathbf{k}_p) \, W_1|\mathbf{k}_1 + \dots + \mathbf{k}_p| = \tag{46}$$
$$W_1(k_1) \dots W_1(k_p) \int d\alpha_1 \dots d\alpha_p \, J_p(\mathbf{k}_1, \dots, \mathbf{k}_p),$$

where W_1 is defined in (14). This result extends the one obtained in Bernardeau (1994) for the 3D dynamics.

At leading order in Perturbation Theory any cumulant of the form $\langle v_1^p v_2^q \rangle_c$ involves only products of such quantities. The sort of commutation rule given in the previous equation implies that these cumulants can be computed without explicitly taking into account the filtering effects. It means that any cumulant of the form $\langle v_1^p v_2^q \rangle_c$ can be built with a *tree shape construction* with two different kinds of end points. Formally the generating function of such cumulants

$$\chi(\lambda_1, \lambda_2) = \sum_{p,q} \frac{\lambda_1^p \lambda_2^q}{p! \, q!} \langle v_1^p v_2^q \rangle_c \tag{47}$$

reads,

$$\chi(\lambda_1, \lambda_2) = \lambda_1 \zeta_J(\tau_1) + \lambda_2 \zeta_J(\tau_2) - \tag{48}$$
$$\frac{\lambda_1}{2} \tau_1 \, \zeta_J'(\tau_1) - \frac{\lambda_2}{2} \tau_2 \, \zeta_J'(\tau_2)$$
$$\tau_1 = \lambda_1 \overline{\xi}_{11} \zeta_J'(\tau_1) + \lambda_2 \overline{\xi}_{12} \zeta_J'(\tau_2) \tag{49}$$
$$\tau_2 = \lambda_1 \overline{\xi}_{12} \zeta_J'(\tau_1) + \lambda_2 \overline{\xi}_{22} \zeta_J'(\tau_2), \tag{50}$$

where $\overline{\xi}_{ij}$ are the second moment of the linear density contrasts between two cells of fixed Lagrangian radii θ_i and θ_j,

$$\overline{\xi}_{ij} \equiv \overline{\xi}_{ij}(\theta_i, \theta_j) = \int \frac{d^2\mathbf{k}}{(2\pi)^2} \, P(k) \, W(k\theta_i) \, W(k\theta_j). \tag{51}$$

They are, for the Lagrangian variables v_i, fixed parameters that depend only on the power spectrum shape (and on the set of cell radii chosen at the beginning). The function ζ_J is the generating function of the angular averages of $J_p(\mathbf{k}_1, \dots, \mathbf{k}_p)$,

$$\zeta_J(\tau) = \sum_{p=0}^{\infty} j_p \frac{\tau^p}{p!}, \quad j_0 = 1 \tag{52}$$

$$j_p = \frac{1}{(2\pi)^p} \int d\alpha_1 \dots d\alpha_p \, J_p(\mathbf{k}_1, \dots, \mathbf{k}_p). \tag{53}$$

Note that $\zeta(\tau) - 1 = 1/\zeta_J(\tau) - 1$ describes the density contrast of a spherical density fluctuation of linear over-density τ for the

2D dynamics. The exact form of ζ_J is therefore known for any cosmological model.

The relation (48) can actually be generalized to an arbitrary number of cells in a straightforward way,

$$\chi(\{\lambda_i\}) = \sum_{i=1}^{n} \lambda_i \zeta_J(\tau_i) - \frac{\lambda_i}{2} \tau_i \, \zeta'_J(\tau_i) \quad (54)$$

$$\tau_i = \sum_{j=1}^{n} \lambda_j \, \bar{\xi}_{ij} \, \zeta'_J(\tau_j). \quad (55)$$

The latter relation can be rewritten in an equivalent way as

$$\sum_{j=1}^{n} C_{ij} \tau_j = \lambda_i \zeta'_J(\tau_i) \quad (56)$$

where C_{ij} is the inverse matrix to $\bar{\xi}_{ij}$. The generating function χ can then be written,

$$\chi(\{\lambda_i\}) = \sum_{i=1}^{n} \lambda_i \, \zeta_J(\tau_i) - \frac{1}{2} \sum_{i,j=1}^{n} C_{ij} \, \tau_i \, \tau_j. \quad (57)$$

It gives the generating function of the reduced volume generating function of an arbitrary number of concentric cells. Note that however the known geometrical properties of the Lagrangian expansion terms do not allow to extend these results to non-concentric cells. Thus, our method actually apply to any filter which is axisymmetric (in general one would need an infinite number of cells but in practice numerical discretization always leads to a finite number of concentric shells). It is worth noting that the relation (55) gives,

$$\sum_j \lambda_j \zeta'_J(\tau_j) \frac{d\tau_j}{d\lambda_i} - \sum_j \tau_j \zeta''_J(\tau_j) \frac{d\tau_j}{d\lambda_i} = \tau_i \zeta'_J(\tau_i) \quad (58)$$

which in turns leads to,

$$\frac{\partial \chi(\{\lambda_i\})}{\partial \lambda_i} = \zeta(\tau_i). \quad (59)$$

4.2. Saddle point approximation and leading order cumulant generating function

In this subsection we explicit the formal relationship between the generating function computed at leading order and the shape of the multivalued density probability distribution function.

The joint PDF is formally given by (this is an extension of Eq. 19)

$$P(v_1, \ldots, v_n) = \int \frac{d\lambda_1}{2\pi i} \cdots \frac{d\lambda_n}{2\pi i} \quad (60)$$

$$\times \exp\left[\chi(\{\lambda_i\}) - \sum_{i=1}^{n} \lambda_i v_i\right].$$

In case of a small variance, the expression of the joint density is obtained through the saddle point approximation. The saddle point conditions read,

$$\frac{\partial \chi}{\partial \lambda_i} = v_i, \quad (61)$$

which gives implicitly the values of λ_i at the saddle point position in terms of v_i. Taking advantage of the property (59), one gets,

$$\zeta_J(\tau_i) = v_i. \quad (62)$$

It implies that with the saddle point position the expression of the joint PDF is (not taking into account prefactors),

$$P_{\text{Lag.}}(v_1, \ldots, v_n) \sim \exp\left[-\frac{1}{2} \sum_{ij} C_{ij} \, \tau_i \, \tau_j\right] \quad (63)$$

with the mapping (62). This is exactly what one would expect for Gaussian initial conditions, τ_i being the linearly extrapolated density contrasts at the chosen scales.

4.3. Lagrangian-Eulerian mapping

To relate Lagrangian and Eulerian space, one uses the same trick as in Bernardeau (1994), that is,

$$P_{\text{Lag.}}\left(v_1 > \frac{1}{\rho_{01}}, \ldots, v_n > \frac{1}{\rho_{0n}}\right) =$$
$$P_{\text{Eul.}}(\rho_1 < \rho_{01}, \ldots, \rho_n < \rho_{0n}). \quad (64)$$

The leading order cumulant generating function can then be obtained by an identification of the exponential term when one uses the saddle point approximation. The variables are however now changed in ρ_i which are related to τ_i with

$$\zeta(\tau_i) = \rho_i, \quad \zeta(\tau_i) = 1/\zeta_J(\tau_i). \quad (65)$$

Moreover the variables ρ_i enter also the expression of the cell correlation coefficients $\bar{\xi}_{ij}$ since they are in Eq. (51) computed for a fixed mass scale and not for a fixed Eulerian space radius. As a result, the coefficient C_{ij} expressed in terms of $\bar{\xi}_{ij}$ should be understood as function of the variable ρ_i through

$$\bar{\xi}_{ii} = \bar{\xi}\left(\rho_i^{1/2} \theta_i\right) \quad (66)$$

$$\bar{\xi}_{ij} = \bar{\xi}\left(\rho_i^{1/2} \theta_i, \rho_j^{1/2} \theta_j\right) \quad (67)$$

where θ_i are all kept fixed.

The cumulant generating function in Eulerian space is obtained also with a saddle point approximation in the computation of

$$\exp\left[\chi_{\text{Eul}}(\{\lambda_i\})\right] = \int d\rho_1 \ldots d\rho_n \, P_{\text{Eul}}(\rho_1, \ldots, \rho_n)$$
$$\times \exp\left(\sum_i \lambda_i \rho_i\right) \quad (68)$$

which leads to,

$$\chi_{\text{Eul}}(\{\lambda_i\}) = \sum_{i=1}^{n} \lambda_i \rho_i - \frac{1}{2} \sum_{i,j=1}^{n} C_{ij} \, \tau_i \, \tau_j \quad (69)$$

with the stationary conditions,

$$\frac{1}{2} \frac{\partial}{\partial \rho_i} \sum_{i,j=1}^{n} C_{ij} \, \tau_i \, \tau_j = \lambda_i \quad (70)$$

where the partial derivatives should then be understood for fixed radius θ_i and λ_i. The relation (69), together with the conditions (70) gives the formal expression of the cumulant generating function in Eulerian space.

The case we are interested in,

$$M_{\mathrm{ap}} = \rho_1 - \rho_2 \qquad (71)$$

if

$$\theta_1 = 1/2, \quad \theta_2 = 1 \qquad (72)$$

corresponds to 2 cells, if M_{ap} is built with the filter (15). Then the generating function for M_{ap} is obtained with a peculiar choice for λ_i,

$$\lambda = \lambda_1 = -\lambda_2. \qquad (73)$$

It is actually convenient to define,

$$y = -\lambda \sigma^2 \qquad (74)$$

and

$$\varphi_{2D}(y) = \varphi_{\mathrm{cyl.}}(y) = -\chi(\lambda)\sigma^2 \qquad (75)$$

where σ^2 is defined by

$$\sigma^2 = \langle M_{\mathrm{ap}}^2 \rangle = \overline{\xi}_{11} + \overline{\xi}_{22} - 2\overline{\xi}_{12}. \qquad (76)$$

With this choice of variable, $\varphi(y)$ does not depend formally on the variance but only on y. To be more specific one has finally,

$$\varphi_{\mathrm{cyl.}}(y) = y\zeta(\tau_1) - y\zeta(\tau_2) + \mathcal{F}(\tau_1, \tau_2) \qquad (77)$$

$$\mathcal{F}(\tau_1, \tau_2) = \frac{\sigma^2}{2[1 - r(\tau_1, \tau_2)]}$$

$$\times \left[\frac{\tau_1^2}{\overline{\xi}_{11}(\tau_1)} + \frac{\tau_2^2}{\overline{\xi}_{22}(\tau_2)} - \frac{2r(\tau_1, \tau_2)\tau_1\tau_2}{\sqrt{\overline{\xi}_{11}(\tau_1)\overline{\xi}_{22}(\tau_2)}} \right], \qquad (78)$$

where $r = \overline{\xi}_{12}/\sqrt{\overline{\xi}_{11}\overline{\xi}_{22}}$, $\overline{\xi}_{11}$ and $\overline{\xi}_{22}$ are considered as function of τ_1 and τ_2 through the variables ρ_1 and ρ_2. the saddle point conditions then read,

$$\frac{\partial \mathcal{F}}{\partial \tau_1} = -y\,\zeta'(\tau_1) \qquad (79)$$

$$\frac{\partial \mathcal{F}}{\partial \tau_2} = y\,\zeta'(\tau_2). \qquad (80)$$

In this case the function $\chi(\lambda)$ can be numerically calculated. We have restricted our calculations to the case where the power spectrum follows a power law behavior with index $n = -1.5$. To do the numerical computations we also use a simplified expression for the 2D spherical collapse dynamics,

$$\zeta(\tau) = (1 + \tau/\kappa)^{-\kappa} \qquad (81)$$

with

$$\kappa = \frac{\sqrt{13} - 1}{2} \approx 1.30. \qquad (82)$$

The resulting function $\varphi_{\mathrm{cyl.}}(y)$ is shown in Fig. 2, together with the functions $\tau_1(y)$ and $\tau_2(y)$.
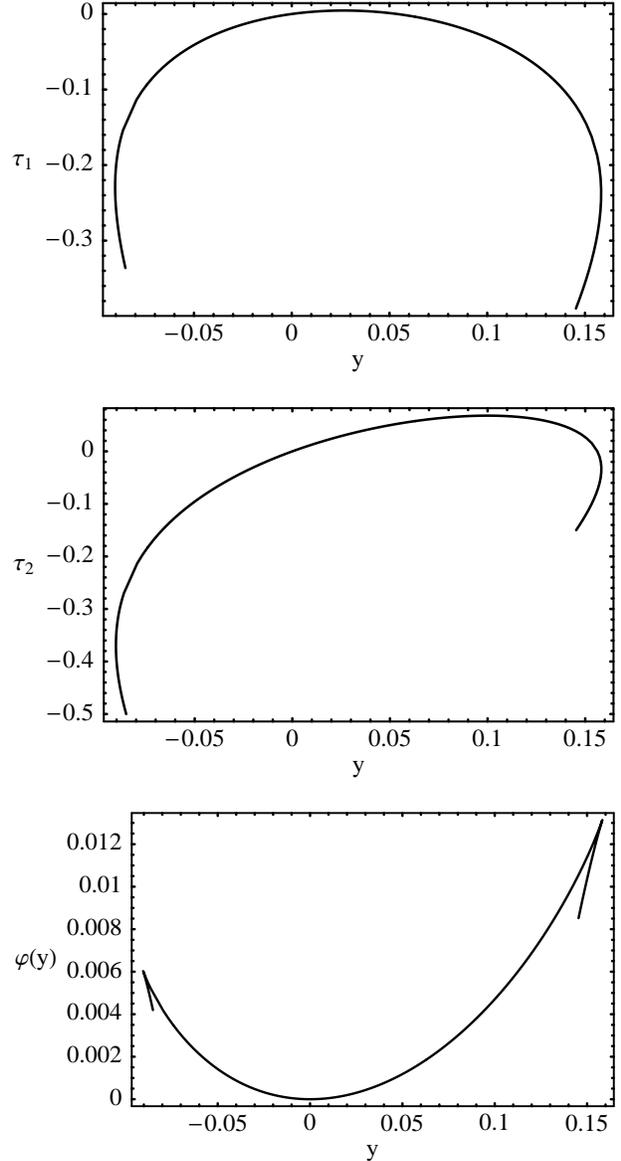

Fig. 2. Shape of the functions $\tau_1(y)$ and $\tau_2(y)$ for the two-cell compensated window function ($y \equiv -\lambda\sigma^2$). The computations have been done for a power law spectrum for $n = -1.5$. The solution for τ has been extended beyond the singularity to show explicitly that the singularities are due to double solution in y.

4.4. Properties of the cumulant generating function

These figures clearly show that the function $\varphi(y)$ has two singularities on the real axis. This is to be compared to what is encountered for counts-in-cells statistics where only one singular point is expected. The numerical resolutions have been extended slightly beyond the singularities to show that they are due to the resolution of the implicit equations in τ that have multiple solution in y. As a result the generic behavior near any of such singularity is

$$\tau(y) \sim t_s (y - y_s)^{1/2}, \qquad (83)$$

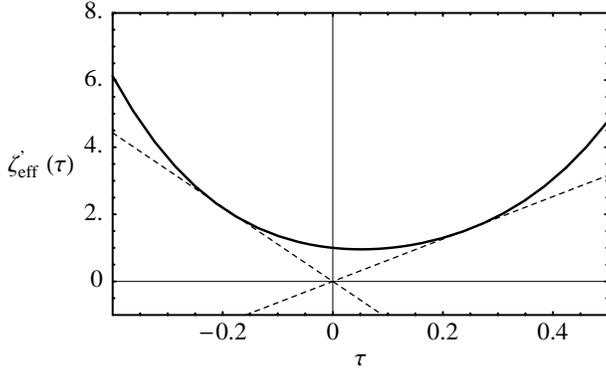$$\varphi_{\mathrm{cyl.}}(y) \sim a_s (y - y_s)^{3/2}. \qquad (84)$$

Fig. 3. Geometrical representation of Eq. (86). The function $\tau(y)$ is given by the intersection of the line $-\tau/y$ with the curve $\zeta'_{\rm eff.}(\tau)$. Singularities appear when both curves are tangential, as shown in the figure.

This behavior directly induces exponential cutoffs for the shape of the density PDF (see Balian & Schaeffer 1989; Bernardeau & Schaeffer 1992). In case of compensated filter, the fact that we obtain 2 singularities, induces two exponential cut-offs on both side of the PDF as it appears clearly on the results presented in Sect. 6 (see also Valageas 2000c).

In a phenomenological way the function $\varphi_{\rm cyl.}(y)$ can be described by an effective vertex generating function $\zeta_{\rm eff.}(\tau)$ so that,

$$\varphi_{\rm cyl.}(y) \,=\, y\,\zeta_{\rm eff.}(\tau) - \frac{1}{2}y\,\tau\,\zeta'_{\rm eff.}(\tau) \tag{85}$$

$$\tau \,=\, -y\,\zeta'_{\rm eff.}(\tau). \tag{86}$$

Numerically the effective vertex generating function is well described by a fifth order polynomial,

$$\zeta_{\rm eff.}(\tau) \,=\, -\tau + 0.843179\,\tau^2 - 5.7511\,\tau^3 + 3.3669\,\tau^4 - \\ 6.3852\,\tau^5 \tag{87}$$

which is regular, the expected singular behavior for $\varphi(y)$ being induced by Eq. (86) (see Fig. 3). Note that $\zeta_{\rm eff.}(\tau)$ can be viewed as a generating function of effective vertices. It implies that for instance the skewness of the 2D (or equivalently cylindrical) compensated filtered density is

$$S_3^{\rm cyl.} = 3 \times 0.843179 \approx 2.52 \tag{88}$$

for such power law spectrum shape. It is however important to have in mind that the shape of $\zeta_{\rm eff.}(\tau)$ as well as the skewness depend on the window function *normalization*. The calculations have been given here for the u_{BV} filter defined in Eq. (15). For the u_S filter, Eq. (12), $S_3^{\rm cyl.}$ for instance would have been about 1.459 times larger, because of the normalization discrepancy between the two filters.

The skewness of $M_{\rm ap}$ is then related to this one through a simple projection factor,

$$S_3^{\rm proj.} = S_3^{\rm cyl.} \frac{\int {\rm d}\mathcal{R}\, F^3 \left[P_0(z)\,\mathcal{D}^{-(n+2)}\right]^2}{\left[\int {\rm d}\mathcal{R}\, F^2\, P_0(z)\,\mathcal{D}^{-(n+2)}\right]^2}. \tag{89}$$

This latter relation is actually valid in both the quasilinear and the nonlinear regime.

5. The nonlinear regime

In the nonlinear regime, there exist no derivations from first principles of the behavior of the high order correlation functions of the cosmic density field. However, hints of its behavior can be found. The *stable clustering ansatz* gives indication on the expected amplitude of the high order correlation functions and how they scale with the two-point one. The hierarchical tree model, and more specifically the *minimal tree model*, allows to build a coherent set of high-order correlation functions.

5.1. The stable-clustering ansatz

The stable clustering ansatz (Peebles 1980) simply states that the high order correlation functions should compensate, in virialized objects, the expansion of the Universe. It gives not only the growth factor of the two-point correlation, but also a scaling relation between the high-order correlation functions.

Expressed in terms of the coefficient S_p -hence of the generating function $\varphi(y)$ defined in (18)- it means that they are independent of time and scale. As a consequence, the knowledge of the evolution of the power-spectrum $P(k)$, or of the two-point correlation function $\bar\xi$, is sufficient to obtain the full PDF of the local density contrast. This property has been checked in numerical simulations by several authors (Valageas et al. 2000; Bouchet et al. 1991; Colombi et al. 1997; Munshi et al. 1999). In particular, the statistics of the counts-in-cells measured in numerical simulations provide an estimate of the generating function $\varphi(y)$ for 3D top-hat filters.

More precisely, in the highly non-linear regime one considers the variable x defined by:

$$x = \frac{1 + \delta_R}{\bar\xi}. \tag{90}$$

Then, using (19), for sufficiently "large" density contrasts the PDF $P(\delta_R)$ can be written as (Balian & Schaeffer 1989):

$$P(\delta_R) = \frac{1}{\bar\xi^2}\, h(x) \tag{91}$$

when

$$\bar\xi \gg 1,\ (1 + \delta_R) \gg \bar\xi^{-\omega/(1-\omega)} \tag{92}$$

where the scaling function $h(x)$ is the inverse Laplace transform of $\varphi(y)$:

$$h(x) = -\int_{-i\infty}^{+i\infty} \frac{{\rm d}y}{2\pi{\rm i}}\, e^{xy}\, \varphi(y). \tag{93}$$

In (92) the exponent ω comes from the behavior of $\varphi(y)$ at large y. Indeed, from very general considerations (Balian & Schaeffer 1989) one expects the function $\varphi(y)$ defined in (18) to behave for 3D top-hat filtering as a power-law for large y:

$$y \to +\infty \,:\, \varphi(y) \sim a\, y^{1-\omega} \quad \text{with } 0 \le \omega \le 1\ ,\ a > 0 \tag{94}$$

and to display a singularity at a small negative value of y,

$$y \to y_s^+ \,:\, \varphi(y) = -a_s\, \Gamma(\omega_s)\, (y - y_s)^{-\omega_s} \tag{95}$$

where we neglected less singular terms (note that this behavior has indeed been observed in the quasilinear regime, Bernardeau 1992). Taking advantage of these assumptions, one obtains (Balian & Schaeffer 1989),

$$x \ll 1 : \quad h(x) \sim \frac{a(1-\omega)}{\Gamma(\omega)} \, x^{\omega-2} \tag{96}$$

$$x \gg 1 : \quad h(x) \sim a_s \, x^{\omega_s-1} \, e^{-x/x_s} \tag{97}$$

with $x_s = 1/|y_s|$. Hence, using (91) we see that the density probability distribution $P(\delta_R)$ shows a power-law behavior from $(1 + \delta_R) \sim \overline{\xi}^{-\omega/(1-\omega)}$ up to $(1 + \delta_R) \sim x_s \overline{\xi}$ with an exponential cutoff above $x_s \overline{\xi}$. It implies in particular that the function $h(x)$ measured in numerical simulations can give rise to constraints on the cumulant generating function from the inverse relation,

$$\varphi(y) = \int_0^\infty \left(1 - e^{-xy}\right) \, h(x) \, \mathrm{d}x \tag{98}$$

Note that $h(x)$ depends on the power-spectrum and, in the absence of a reliable theory for describing the nonlinear regime, it has to be obtained from numerical simulations. This is the case in particular for the evolution of the two-point correlation function, or equivalently of the power-spectrum. To this order we use the analytic formulae obtained by Peacock & Dodds (1996) from fits to N-body simulations.

Note that the relation (93) holds independently of the stable-clustering ansatz. However, if the latter is not realized the generating function $\varphi(y)$ depends on time (and scale). Then, most of the results we obtain in the next sections still hold but one needs to take into account the evolution with redshift of $\varphi(y)$. That would be necessary in particular if one wants to describe the transition from the quasilinear regime to the strongly nonlinear regime. In the following we assume that the stable-clustering ansatz is valid, so that $\varphi(y)$ is time-independent. As mentioned above this is consistent with the results of numerical simulations.

5.2. Minimal tree-model

If one is interested in the statistics of the top-hat filtered convergence, it is reasonable to assume that (Valageas 2000a,b),

$$\varphi_{\mathrm{cyl.}}(y) \approx \varphi_{3D}(y). \tag{99}$$

In case of the aperture mass statistics however the filtering scheme is too intricate (with both positive and negative weights) to make such an assumption, and in particular the resulting values for S_p depend crucially on the geometrical dependences of the p-point correlation functions. We are thus forced to adopt a specific model for the correlation functions, and the one we adopt is obviously consistent with the stable-clustering ansatz.

A popular model for the p-point correlation functions in the non-linear regime is to consider a "tree-model" (Schaeffer 1984; Groth & Peebles 1977) where ξ_p is expressed in terms of products of ξ_2 as:

$$\xi_p(\mathbf{r}_1, ..., \mathbf{r}_p) = \sum_{(\alpha)} Q_p^{(\alpha)} \sum_{t_\alpha} \prod_{p-1} \xi_2(\mathbf{r}_i, \mathbf{r}_j) \tag{100}$$

where (α) is a particular tree-topology connecting the p points without making any loop, $Q_p^{(\alpha)}$ is a parameter associated with the order of the correlations and the topology involved, t_α is a particular labeling of the topology (α) and the product is made over the $(p-1)$ links between the p points with two-body correlation functions. A peculiar case of the models described by (100) is the "minimal tree-model" (Bernardeau & Schaeffer 1992, 1999; Munshi et al. 1999) where the weights $Q_p^{(\alpha)}$ are given by:

$$Q_p^{(\alpha)} = \prod_{\text{vertices of } (\alpha)} \nu_q \tag{101}$$

where ν_q is a constant weight associated to a vertex of the tree topology with q outgoing lines. Then, one can derive the generating function $\varphi(y)$, defined in (18), or the coefficients S_p, from the parameters ν_p introduced in (101) which completely specify the behavior of the p-point correlation functions.

In this case the cumulant generating function is given for 3D filtering by,

$$\chi(\lambda) = \sum_{p=1}^\infty \frac{\lambda^p}{p!} \int \mathrm{d}^3\mathbf{r}_1 .. \mathrm{d}^3\mathbf{r}_p \, w(\mathbf{r}_1)..w(\mathbf{r}_p) \, \xi_p(\mathbf{r}_1, .., \mathbf{r}_p) \tag{102}$$

where w corresponds to the filter choice. In the case of the minimal tree-model, where the p-point correlation functions are defined by the coefficients ν_q from (100) and (101), it is possible to obtain a simple implicit expression for the function $\chi(\lambda)$ (see Bernardeau & Schaeffer 1992; Jannink & des Cloiseaux 1987):

$$\chi(\lambda) = \lambda \int \mathrm{d}^3\mathbf{r} \, w(\mathbf{r}) \left[\zeta[\tau(\mathbf{r})] - \frac{\tau(\mathbf{r})\zeta'[\tau(\mathbf{r})]}{2} \right] \tag{103}$$

$$\tau(\mathbf{r}) = \lambda \int \mathrm{d}^3\mathbf{r}' \, w(\mathbf{r}') \, \xi_2(\mathbf{r}, \mathbf{r}') \, \zeta'[\tau(\mathbf{r}')] \tag{104}$$

where the function $\zeta(\tau)$ is defined as the generating function for the coefficient ν_p,

$$\zeta(\tau) = \sum_{p=0}^\infty \frac{(-1)^p}{p!} \, \nu_p \, \tau^p \quad \text{with} \quad \nu_0 = \nu_1 = 1. \tag{105}$$

The function $\chi(\lambda)$ obviously depends on the choice of filter through the function w. For a top-hat filter, it would simply be a characteristic function normalized in such a way that

$$\int \mathrm{d}^3\mathbf{r} \, w(r) = 1. \tag{106}$$

A simple "mean field" approximation which provides very good results in case of top-hat filter (Bernardeau & Schaeffer 1992) is to integrate $\tau(\mathbf{r})$ over the volume V in the second line of the system (103) and then to approximate $\tau(\mathbf{r})$ by a constant τ. This leads to the simple system:

$$\varphi_{3D}(y) = y \left[\zeta(\tau) - \frac{\tau \, \zeta'(\tau)}{2} \right] \tag{107}$$

$$\tau = -y \, \zeta'(\tau) \tag{108}$$

Then, the singularity of $\varphi(y)$, see (95), corresponds to the point where the $|\mathrm{d}y/\mathrm{d}\tau|$ vanishes. Note that $\zeta(\tau)$ is regular at this point and that the singularity is simply brought about by the form of the implicit system (108) as observed in Bernardeau & Schaeffer (1992). Making the approximation (107-108) for both $\varphi_{3D}(y)$ and $\varphi_{\mathrm{cyl.}}(y)$ leads to the approximation (99) which is thus natural for the minimal tree model.

In the case of a compensated filter such a simple mean field approximation however cannot be done. It is in particular due to the fact that the weights given to τ then strongly depend on the radius distance. Before we go to this point we need first to take into account the projection effects.

5.3. Projection effects for the minimal tree-model

As noted in Tóth et al. (1989) and analyzed in detail in Valageas (2000b), we know that the tree structure assumed for the 3D correlation functions is preserved (except for one final integration along the line-of-sight) for the projected density. Indeed, inserting (100) in (24) we obtain:

$$\langle \delta_{\mathrm{proj.}}(\boldsymbol{\vartheta}_1)..\delta_{\mathrm{proj.}}(\boldsymbol{\vartheta}_p)\rangle_c = \sum_{(\alpha)} Q_p^{(\alpha)} \sum_{t_\alpha} \int_0^{\mathcal{R}_s} \mathrm{d}\mathcal{R}_1 \ F^p$$
$$\times \int_{-\infty}^{\infty} \prod_{i=2}^{p} \mathrm{d}\mathcal{R}_i \prod_{p-1} \xi_2(\mathbf{x}_a, \mathbf{x}_b) \quad (109)$$

where we noted $\mathbf{x}_a = (\mathcal{R}_a, \mathcal{D}_1 \boldsymbol{\vartheta}_a)$. It can be noted that in the small angle approximation the weight applied to each diagram depends on their order p only and not on their geometrical decompositions. As a consequence the projected $p-$point correlation function can be written,

$$\langle \delta_{\mathrm{proj.}}(\boldsymbol{\vartheta}_1) \ldots \delta_{\mathrm{proj.}}(\boldsymbol{\vartheta}_p)\rangle_c =$$
$$\int_0^{\mathcal{R}_s} \mathrm{d}\mathcal{R} \ F^p \ \omega_p(\boldsymbol{\vartheta}_1, \ldots, \boldsymbol{\vartheta}_p; z), \quad (110)$$

where the two-dimensional $p-$point functions $\omega_p(\boldsymbol{\vartheta}_1, ..., \boldsymbol{\vartheta}_p; z)$ have the same tree-structure as the three-dimensional $p-$point correlation functions ξ_p,

$$\omega_p(\boldsymbol{\vartheta}_1, \ldots, \boldsymbol{\vartheta}_p; z) = \sum_{(\alpha)} Q_p^{(\alpha)} \sum_{t_\alpha} \prod_{p-1} \omega_2(\boldsymbol{\vartheta}_a, \boldsymbol{\vartheta}_b; z) \quad (111)$$

with:

$$\omega_2(\boldsymbol{\vartheta}_1, \boldsymbol{\vartheta}_2; z) = \int \frac{\mathrm{d}^2\mathbf{k}}{(2\pi)^2} \ P(k, z) \ J_0 \left(k\mathcal{D}|\boldsymbol{\vartheta}_1 - \boldsymbol{\vartheta}_2|\right). \quad (112)$$

Here J_0 is the Bessel function of order 0. For convenience we also note $\overline{\omega}_2(z)$ the angular average of $\omega_2(\boldsymbol{\vartheta}_1, \boldsymbol{\vartheta}_2; z)$,

$$\overline{\omega}_2(z) = \int \mathrm{d}^2\boldsymbol{\vartheta}_1 \mathrm{d}^2\boldsymbol{\vartheta}_2 \ U(\boldsymbol{\vartheta}_1) \ U(\boldsymbol{\vartheta}_2) \ \omega_2(\boldsymbol{\vartheta}_1, \boldsymbol{\vartheta}_2; z), \quad (113)$$

which, expressed in terms of the power spectrum gives,

$$\overline{\omega}_2(z) = \int_0^{\infty} \frac{\mathrm{d}^2\mathbf{k}}{(2\pi)^2} P(k) \ W^2(k\mathcal{D}\theta). \quad (114)$$

Thus, we see that the correlation functions of the projected density $\delta_{\mathrm{proj.}}$ itself do not show an exact tree-structure as the underlying 3D correlation functions ξ_p. Nevertheless, as seen in (110) they are given by one simple integration along the line-of-sight of the 2D $p-$point functions ω_p which exhibit the *same tree-structure* as their 3D counterparts ξ_p. This means that we can still use the techniques developed to deal with such tree-models. In particular, in the case of the minimal tree-model (101) we will be able to take advantage of the resummation (103-104).

Once again, it is interesting to note that for power-law spectra, $P(k) \propto k^n$, the angular and the redshift dependences of ω_p can be factorized so that the correlation functions of the projected density $\delta_{\mathrm{proj.}}$ itself now exhibit a (new) tree-structure. Then, the 2-point function reads,

$$\langle \delta_{\mathrm{proj.}}(\boldsymbol{\vartheta}_1)\delta_{\mathrm{proj.}}(\boldsymbol{\vartheta}_2)\rangle = |\boldsymbol{\vartheta}_1 - \boldsymbol{\vartheta}_2|^{-(n+2)}$$
$$\times \int_0^{\infty} \frac{\mathrm{d}^2\mathbf{l}}{(2\pi)^2} \ l^n \ J_0(l) \int \mathrm{d}\mathcal{R} \ F^2(\mathcal{R}) \ \frac{P_0}{k_0^n} \ \mathcal{D}^{-(n+2)} \quad (115)$$

while the high-order $p-$point functions $\langle \delta_{\mathrm{proj.}}(\boldsymbol{\vartheta}_1)..\delta_{\mathrm{proj.}}(\boldsymbol{\vartheta}_p)\rangle_c$ follow the tree-structure (100) with the projected weights $Q_{p,\,\mathrm{proj.}}^{(\alpha)}$:

$$Q_{p,\,\mathrm{proj.}}^{(\alpha)} = Q_p^{(\alpha)} \frac{\int \mathrm{d}\mathcal{R} \ F^p \left[P_0(z) \ \mathcal{D}^{-(n+2)}\right]^{p-1}}{\left[\int \mathrm{d}\mathcal{R} \ F^2 \ P_0(z) \ \mathcal{D}^{-(n+2)}\right]^{p-1}}. \quad (116)$$

Note that the relation $Q_p^{(\alpha)} \leftrightarrow Q_{p,\,\mathrm{proj.}}^{(\alpha)}$ depends on the slope n of the power-spectrum. On the other hand, if the initial tree-model for the 3D correlation functions is the minimal tree-model (101) we can see that the projected tree-structure (116) is *not an exact minimal* tree-model[1] which would be expressed in terms of a new generating function $\zeta_{\mathrm{proj.}}(\tau)$. In other words $\varphi_{\mathrm{proj.}}(y)$ cannot be built from a tree structure whereas $\varphi_{\mathrm{cyl.}}(y)$ can, and with the *same* vertex generating function $\zeta(\tau)$ defined in (105).

As a consequence, in the nonlinear regime, the relation (34) is to be used with,

$$\varphi_{\mathrm{cyl.}}(y) = y \int \mathrm{d}^2\vartheta \ U(\boldsymbol{\vartheta}) \left[\zeta[\tau(\boldsymbol{\vartheta})] - \frac{\tau(\boldsymbol{\vartheta})\zeta'[\tau(\boldsymbol{\vartheta})]}{2}\right] \quad (117)$$

$$\tau(\boldsymbol{\vartheta}) = -y \int \mathrm{d}^2\vartheta' \ U(\boldsymbol{\vartheta}') \ \frac{\omega_2(\boldsymbol{\vartheta}, \boldsymbol{\vartheta}'; z)}{\overline{\omega}_2(z)} \ \zeta'[\tau(\boldsymbol{\vartheta}')] \quad (118)$$

where $\zeta(\tau)$ is the 3D vertex generating function. Note that this function depends on z through $\omega_2(\boldsymbol{\vartheta}, \boldsymbol{\vartheta}'; z)$ and $\overline{\omega}_2(z)$. Note also that in $y = 0$ the expansion of the generating function $\varphi_{\mathrm{cyl.}}(y)$ is $\varphi_{\mathrm{cyl.}}(y) = -y^2/2 + \ldots$.

We have computed the resulting shape of the generating function in such a model for various cases. For comparison with the previous quasi-linear case we assume here the power spectrum to follow a power law behavior with index $n = -1.5$. The vertex generating function is assumed to be given by

$$\zeta(\tau) = (1 + \tau/\kappa)^{-\kappa} \quad (119)$$

---

[1] This is due to the fact that the numerator in the r.h.s. of (116) cannot be factorized in the form $A \ B^{p-1}$. A simple way to check that $Q_{p,\,\mathrm{proj.}}^{(\alpha)}$ cannot be written in terms of new parameters $\nu_{q,\,\mathrm{proj.}}$ as in (101) is to consider the "snake" topology where $Q_p^{(\mathrm{snake})} = \nu_1^2 \ \nu_2^{p-2}$.
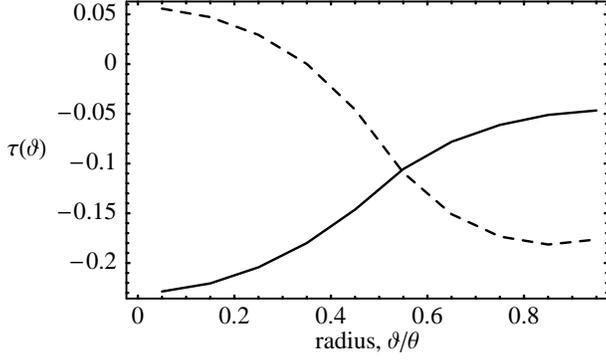
Fig. 4. Profile of the τ function as a function of the angular radius. The two plots correspond to the two singularities, y_{s-} for the solid line and y_{s+} for the dashed line.

with $\kappa \approx 0.5$ (in the parameterization of ζ we followed the traditional notation and used κ as a simple free parameter. It is not to be confused with the local convergence). In Fig. 4 we present typical profiles obtained for $\tau(\vartheta)$. We see that it is regular in ϑ. In particular it does not exhibit discontinuities nor abnormal behavior near the singular values of y. We also found that the results we obtain are very robust regarding to the number of shells used to describe the integral in ϑ: with 2 cells only the description of $\varphi_{\mathrm{cyl.}}$ is already very accurate.

The choice of the value of κ in (119) relies a priori on numerical results. The EPT (Colombi et al. 1997) or more convincingly the HEPT (Scoccimarro & Frieman 1999) provide however a convenient frame which can be used to predict the value of κ. This can be done for instance by identifying the predicted values for the skewness both from the form (119) and HEPT. Indeed in our model we have,

$$S_3(\kappa) = 3\frac{(1+\kappa)}{\kappa} \tag{120}$$

whereas, in HEPT, S_3 is related to the initial power spectrum index,

$$S_3^{\mathrm{HEPT}}(n) = 3\frac{4-2^n}{1+2^{n+1}}, \tag{121}$$

which leads to,

$$\kappa \approx \frac{\left(1+2^{1+n}\right)}{3\left(1-2^n\right)}. \tag{122}$$

In the numerical applications presented in the following we will use this scheme. In particular, $n = -1.5$ leads to $\kappa = 0.88$. On the other hand, at the angular scale $\theta = 4'$ which we consider below the local slope of the linear power-spectrum is $n \simeq -2.2$ which leads to $\kappa \simeq 0.6$.

The properties of $\varphi_{\mathrm{cyl.}}(y)$ we get in this regime are very similar to those obtained for the quasilinear regime. In particular we found that the function $\varphi_{\mathrm{cyl.}}(y)$ exhibits 2 singular points on the real axis. As for the quasilinear regime this behavior is due to the implicit equation in τ and not to peculiar choice of the vertex generating function. In Table 1 we summarize the parameters that describe the singularities of $\varphi_{\mathrm{cyl.}}(y)$ in different regimes.
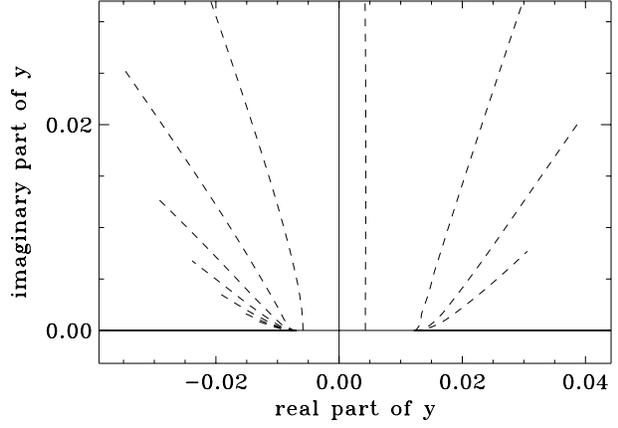

Fig. 5. Integration paths in the y complex plane. The paths (dashed lines) are dynamically built so that the argument of the exponential in Eq. (124) is always a negative real number. The thick half straight lines represent the locations of the non-analytic parts of $\varphi_{\mathrm{proj.}}(y)$ in this plane. Of course, the paths must not cross these branch cuts.

It appears, as expected, that the singularities are closer to the origin. This is to be expected since the nonlinearities contained in $\varphi_{\mathrm{cyl.}}(y)$ are stronger in the nonlinear regime compared to the quasilinear regime.

Similarly to the quasilinear regime it is also possible to define an effective vertex generating function from which $\varphi_{\mathrm{cyl.}}(y)$ can be built and which reproduces its singular points,

$$\zeta_{\mathrm{eff.}}(\tau) = -\tau + 1.4966\,\tau^2 - 11.6982\,\tau^3 + 21.528\,\tau^4 - \\ 77.1899\,\tau^5. \tag{123}$$

The result given here has been obtained for $\kappa = 0.88$ in Eq. (119).

6. Statistics of the aperture mass M_{ap}

It now suffices to plug the numerical expressions we have obtained for $\varphi_{\mathrm{cyl.}}(y)$ in (34) to get the shape of the M_{ap} PDF. More precisely we have,

$$P(M_{\mathrm{ap}})\mathrm{d}M_{\mathrm{ap}} = |\kappa_{\mathrm{min}}|\,\mathrm{d}M_{\mathrm{ap}} \int \frac{\mathrm{d}y}{2\pi\mathrm{i}\sigma^2}$$
$$\times \exp\left[-\frac{|\kappa_{\mathrm{min}}|^2\varphi_{\mathrm{proj.}}(y)}{\sigma^2} + \frac{y|\kappa_{\mathrm{min}}|M_{\mathrm{ap}}}{\sigma^2}\right]. \tag{124}$$

where σ is the variance of the aperture mass.

In (124) the integral over y has to be made in the complex plane. The integration path in the y plane is built in such a way that the argument of the exponential is always a real negative number thus avoiding oscillations (see Fig. 5). Moreover, one must make sure that the integration path does not cross the branch cuts of $\varphi_{\mathrm{cyl.}}(y)$. The singularities of $\varphi_{\mathrm{cyl.}}(y)$ induce non-analytic parts for $\varphi_{\mathrm{proj.}}(y)$ as well. They are located at positions,

$$y > y_{s+}^{\mathrm{proj}} \quad \text{and} \quad y < y_{s-}^{\mathrm{proj}} \tag{125}$$

with

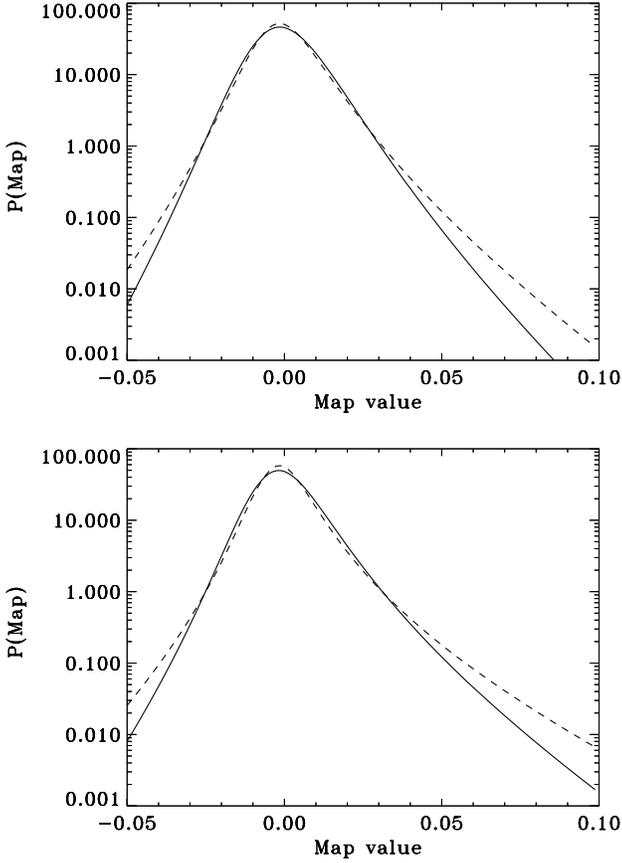$$y_{s\pm}^{\mathrm{proj}} = y_{s\pm}/\max[F(\mathcal{R})\psi(\mathcal{R})] \tag{126}$$

Fig. 7. Same as previously with the nonlinear model but with cell radius ratio of 10 instead of 2.

Table 1. Values of $S_3^{\mathrm{cyl.}}$ and singularity positions of $\varphi_{\mathrm{cyl.}}(y)$ for U_{BV} filter.

	$S_3^{\mathrm{cyl.}}$	y_{s-}	y_{s+}	a_{s-}	a_{s+}
quasi-linear, $n = -1.5$	2.53	-0.092	0.159	1.20	0.74
non-linear, $\kappa = 1.0$, $n = -1.5$	4.19	-0.062	0.130	0.85	0.41
non-linear, $\kappa = 0.88$, $n = -1.5$	4.49	-0.057	0.121	0.83	0.40
non-linear, $\kappa = 0.50$, $n = -1.5$	6.32	-0.040	0.084	0.65	0.31

Fig. 6. Shape of the one-point PDF of the aperture mass from the quasi-linear regime model (top panel) and in the non-linear regime (bottom panel). The sources are at redshift unity, the variance of M_{ap} is 0.01, for the filter given by Eq. 15. the solid lines correspond to Einstein-de Sitter case, the dashed lines to flat universe with $\Omega_{\mathrm{m}} = 0.3$.

where the maximum value of $F(\mathcal{R})\psi(\mathcal{R})$ is taken along the line-of-sight (and is indeed finite). As noticed in Valageas (2000a) the exponent ω_s of the singularity of $\varphi_{\mathrm{cyl.}}(y)$ (as defined in (95)) leads to the exponent $\omega_s - 1/2$ for the projected generating function $\varphi_{\mathrm{proj.}}(y)$. However, in both the quasi-linear and highly non-linear regimes we have $\omega_s = -3/2$, see (84). In this case, as shown in App. A, for $y \to y_{s\pm}^{\mathrm{proj}}$ the singularity is of the form $\varphi_{\mathrm{proj.}}(y) \sim (y - y_{s\pm}^{\mathrm{proj}})^2 \ln |y - y_{s\pm}^{\mathrm{proj}}|$.

The existence of these branch cuts is directly responsible for two exponential cut-offs in the shape of the PDF of M_{ap},

$$P(M_{\mathrm{ap}}) \sim \exp\left(\frac{|\kappa_{\mathrm{min}}| M_{\mathrm{ap}}}{\sigma^2} y_{s\pm}^{\mathrm{proj}} \right). \tag{127}$$

It can be noted that the Ω dependence of κ_{min} will induce a strong Ω dependence in the position of the exponential cut-offs. The variation of κ_{min} with Ω is thus to be compared with the theoretical uncertainties on $y_{s\pm}$.

6.1. The PDF shape

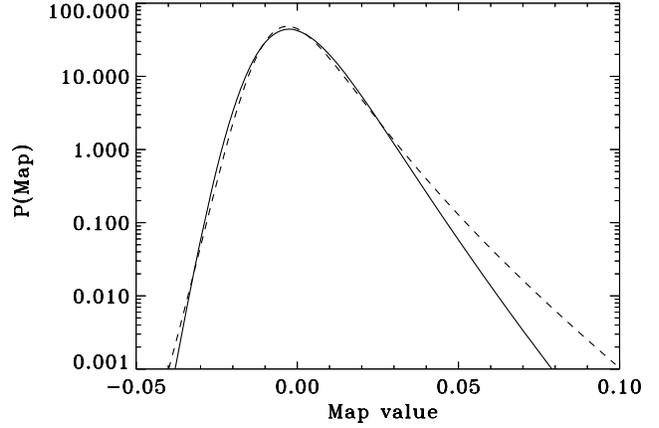In Figs. 6 we present the resulting shape of the one point PDF obtained for different cases. They have been obtained from the parameterization of $\varphi_{\mathrm{cyl.}}(y)$ described in the previous sections. In particular we assume a power law spectrum with index $n = -1.5$. The variance adopted for the plots is $\sigma = 0.01$. In these investigations we did not try to put a realistic source distribution, but we assume all the sources to be at redshift unity. However, all our results can be extended in a straightforward fashion for any redshift distribution of the sources (the latter is simply absorbed by a redefinition of the selection function $F(\mathcal{R})$). Note also that we present the PDF for the correctly normalized aperture mass M_{ap}, that is without dividing the local convergence by κ_{min}. We can check in Fig. 6 that the tails of the PDF are stronger in the non-linear regime than in the quasi-linear regime independently of the variance σ (which is the same in both plots). This is related to the smaller values of the singularities $|y_{s\pm}^{\mathrm{proj}}|$ in the non-linear case, as shown by the expression (127). Of course, this is due to the smaller value of the singularity $|y_s|$ of the 3D density field in the non-linear regime (in a similar fashion the coefficients S_p are larger).

In Fig. 7 we show that the positions of the cut-off depend crucially on the window shape. In particular it is clear that when the disc radius ratio is larger the PDF is more asymmetric and bears more resemblance with the κ-PDF for a top-hat window function. Indeed, when the inner disk is much smaller than the outer radius the fluctuations of $M_{\mathrm{ap}} = \kappa_1 - \kappa_2$ are dominated by those of the convergence κ_1 which corresponds to this small inner window while κ_2 which is governed by larger scales shows lower amplitude fluctuations.
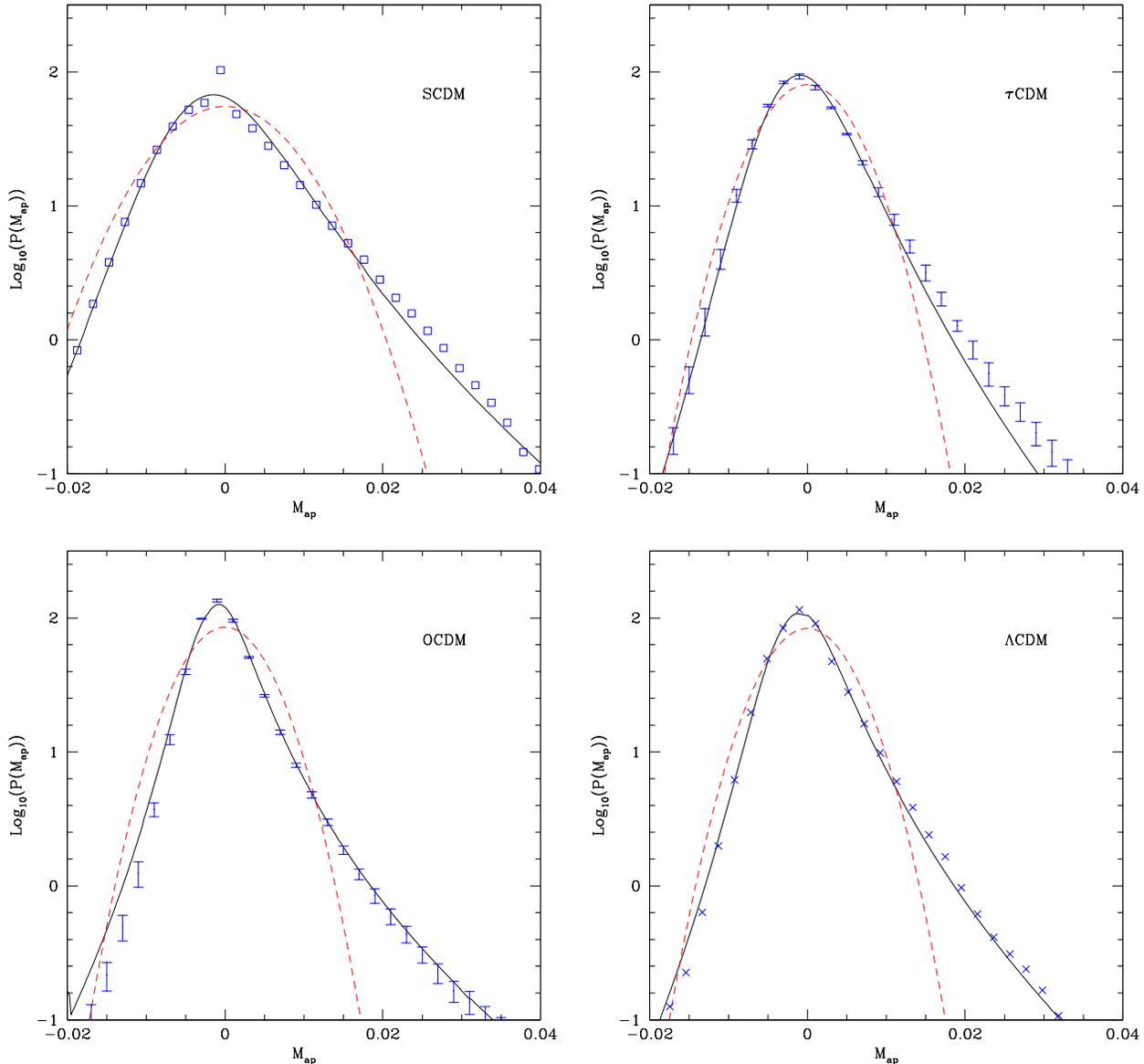
Fig. 8. The aperture mass PDF for a source at redshift $z_s = 1$ for 4 cosmologies and with the angular window $\theta = 4'$. The dashed line shows the Gaussian which has the same variance. The points show the results of N-body simulations from Jain et al. (2000). Results for sCDM and ΛCDM models have been directly taken from Reblinsky et al. (1999).

6.2. The Ω_m dependence of the PDF

It has been stressed in the literature (e.g., Bernardeau et al. 1997) that the non-Gaussian properties of the convergence maps are expected to exhibit a strong Ω_m dependence. This is due in particular to the normalization factor. Such dependence is apparent in κ_min that depends crucially on the value of Ω_m. This property naturally extends to the shape of the one-point PDF. In particular it is important to have in mind that the Ω_m dependence is negligible in $\varphi_\mathrm{cyl.}(y)$ (for a fixed shape of the power spectrum). The Ω_m dependence is therefore entirely contained in the projection effect through the shape and amplitude of the efficiency function.

In Fig. 6 we show how low values of Ω_m amplify the non-Gaussian features contained in the PDF. Whether such a pa-

rameter can be constrained more efficiently with the PDF than with simply the local skewness is not yet clear. Such a study is however beyond the objective of this paper and is left for further works.

6.3. Comparison with numerical simulations

Finally, we compare our predictions for the PDF $P(M_\mathrm{ap})$ of the aperture mass M_ap with the results of N-body simulations (Jain et al. 2000) in Fig. 8. *Note that for all these comparisons we exclusively use the u_S filter.* We consider the cosmological models defined in Table 2: a standard CDM (SCDM) and a τCDM scenario in a critical density universe, a low-density open universe (OCDM) and a low-density flat universe with a

Table 2. Cosmological models and results obtained with U_S filter. The sixth and seventh lines show the variance and the skewness of $P(M_{\rm ap})$ from numerical simulations (Jain et al. 2000). Results for sCDM and ΛCDM models have been directly taken from Reblinsky et al. (1999) and have been obtained with one realization only. The eight and ninth lines show the reconstructed PDF properties.

	sCDM	τCDM (5 realizations)	OCDM (7 realizations)	ΛCDM
$\Omega_{\rm m}$	1	1	0.3	0.3
Ω_Λ	0	0	0	0.7
H_0 [km/s/Mpc]	50	50	70	70
σ_8	0.6	0.6	0.85	0.9
Γ	0.5	0.21	0.21	0.21
$\sigma_{M_{\rm ap}}, \theta = 4'$	0.00730	0.00542 ± 0.00017	0.00449 ± 0.00017	0.00495
$s_3^{M_{\rm ap}}, \theta = 4'$	159	$258. \pm 38.$	$545. \pm 30.$	347
$\sigma_{M_{\rm ap}}, \theta = 4'$	0.00721	0.00497	0.00469	0.00477
$s_3^{M_{\rm ap}}, \theta = 4'$	148	180	395	300

non-zero cosmological constant (ΛCDM). Here Γ is the usual shape parameter of the power-spectrum. We use the fit given by Bardeen et al. (1986) for $P(k)$. We only consider the weak lensing distortions which affect a source at redshift $z_s = 1$, with angular window characteristic scale $\theta = 4'$.

In the numerical calculations, we discretize the integral (34) over redshift and we solve for the system (117 - 118). That is we take into account the redshift dependence of the generating function $\varphi_{\rm cyl.}(y)$. Moreover, we use the relation (122) to get the value of the parameter κ, where for n we take the local slope of the linear-power spectrum at the wavenumber $k = 2/(\mathcal{D}(z_s/2)\theta)$. This corresponds to the Fourier modes which are probed by the filter of angular radius θ, see Fig. 1. For $\theta = 4'$ we obtain $n \simeq -2.2$ and $\kappa \simeq 0.6$.

First, we can check in Fig. 8 that we recover the right trend for $P(M_{\rm ap})$, with two asymmetric tails for large $|M_{\rm ap}|$. In particular, the exponential cutoff is stronger for negative values of the aperture mass than for positive values. We can also note that the PDF is significantly different from a Gaussian as it shows a clear exponential cutoff, much smoother than the Gaussian falloff, especially for large positive $M_{\rm ap}$. On the other hand, we note that Reblinsky et al. (1999) obtained a good match to the tail of the PDF $P(M_{\rm ap})$ using a description of the density field as a collection of virialized halos (Kruse & Schneider 1999). However, such a method is restricted to the far tail of the PDF (large positive $M_{\rm ap}$) while our approach provides in principle a model for the full PDF $P(M_{\rm ap})$. There seems to be a small discrepancy with the simulations for the τCDM scenario. It is not clear whether this is due to a limitation of HEPT or of our formulation. To clarify this problem one should test the statistics of the 3D density field and of the projected density in the same simulation. However, this is beyond the scope of our paper. Nevertheless, the overall agreement appears to be quite reasonable. Note that the shape of the PDF is governed by only one parameter κ, which is uniquely related to the local slope of the power-spectrum, independently of scale and of the cosmology. On the other hand, the inaccuracy of the numerical simulations in the tail of the PDF might be somewhat underestimated.

In order to see more clearly the difference of the aperture mass PDF $P(M_{\rm ap})$ with respect to the Gaussian we display
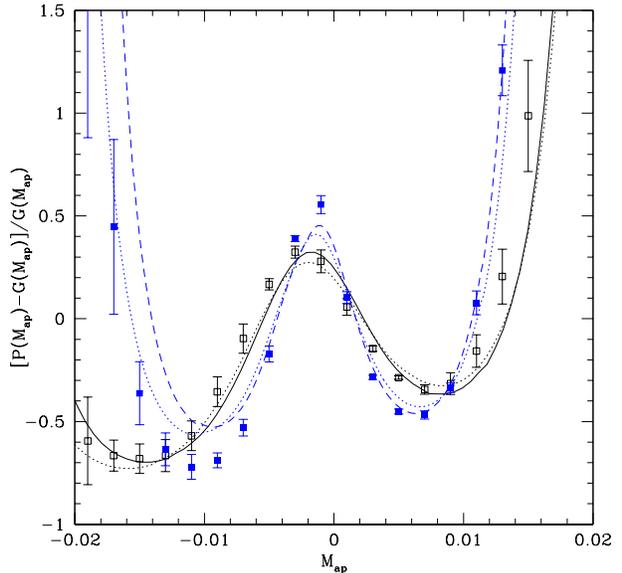

Fig. 9. The relative difference $[P(M_{\rm ap}) - G(M_{\rm ap})]/G(M_{\rm ap})$ of the aperture mass PDF $P(M_{\rm ap})$ with respect to the Gaussian $G(M_{\rm ap})$. The variance of the Gaussian is taken from the simulations. As in Fig. 8 we consider a source at redshift $z_s = 1$ with the angular window $\theta = 4'$. We display our results for the τCDM (solid line) and OCDM (dashed line) cosmologies. The dotted lines correspond to the same cosmologies with $\kappa = 0.88$ (see main text). The points show the results of N-body simulations from Jain et al. (2000).

in Fig. 9 the relative difference $P(M_{\rm ap})/G(M_{\rm ap}) - 1$. Here $G(M_{\rm ap})$ is the Gaussian with the same variance as the numerical simulations. We can check that we recover a reasonable agreement with the numerical results, since Fig. 9 is directly related to Fig. 8. To get an estimate of the sensivity of our predictions with respect to the parameterization (119) and (122) we also plot in Fig. 9 our results for the same cosmologies when we use $\kappa = 0.88$ (this would correspond to an initial power spectrum index $n = -1.5$) in (122). We can see in the figure that our predictions are not too sensitive to κ (for reasonable values of κ) within the range $-0.015 < M_{\rm ap} < 0.015$ (the difference would look even smaller in Fig. 8). In particular, the variation with κ

of our results is much smaller than the difference between both cosmologies. This suggests that one could use the deviation of the PDF with respect to a Gaussian to estimate the cosmological parameters. A well-known tool to measure this signature is the skewness but one could devise other statistics which would take advantage of the expected shape of the PDF to maximize their dependence on cosmology. However, such a study is beyond the scope of this article. We can see in Table 2 that we underestimate somewhat the skewness of $P(M_{\mathrm{ap}})$. However, it is not clear whether this is due to the parameterization (119) or to the use of HEPT in (122). We note that the tail of $P(M_{\mathrm{ap}})$ for large negative values of M_{ap} appears to be slightly more sensitive to κ than the tail at positive M_{ap}. This could be related to the fact that the behaviour of $P(M_{\mathrm{ap}})$ for $M_{\mathrm{ap}} < -\sigma_{M_{\mathrm{ap}}}$ is more sensitive to the detailed properties of the $p-$point correlation functions (see Valageas 2000c for a study of this point).

Finally, we note that although $\theta = 4'$ corresponds to nonlinear scales it is not very far from the quasi-linear regime. However, the aperture mass M_{ap} probes the non-linear density field for filters with larger angular scale than the convergence κ. Indeed, since the aperture mass involves compensated filters the contribution from low-k modes is strongly suppressed (see Fig. 1) so that $P(M_{\mathrm{ap}})$ is governed by the properties of the density field at the comoving wavenumber $k \sim 2/(\mathcal{D}\theta)$. In contrast, the convergence κ shows a more important contribution from larger wavelengths which implies that in order to probe nonlinear scales only one must set the filter size θ farther away into the small-scale non-linear regime. This also means that in principle the aperture mass could be a more convenient tool than the convergence since it should be easier to separate the non-linear and quasi-linear regimes, while for an important range of angular scales the convergence should be sensitive to the transitory regime between both domains. However, a possible caveat is that the statistics of the aperture mass depend on the detailed behaviour of the $p-$point correlation functions (and not on their average over spherical cells only), and therefore requires a better understanding of them.

As discussed above, this property of the aperture mass to probe a narrow range of wavenumbers makes it easier to avoid the intermediate regime as one can select observation windows which are either in the quasi-linear or in the strongly non-linear regime. However, it would clearly be interesting to obtain a model which would also cover this transitory range. Unfortunately, this is rather difficult as one cannot use the simplifications which appear in the two extreme regimes. An alternative to a rigorous calculation would be to use an ad-hoc parameterization which would smoothly join the quasi-linear regime to the highly non-linear regime, for instance in the spirit of HEPT as described in van Waerbeke et al. (2000b) for the skewness of the convergence (note that our model for non-linear scales is based on a simple ansatz which is not rigorously derived). However, although the quasi-linear and strongly non-linear regimes share the same gross features, like the relation (34) which describes the projection effects, their detailed properties are different. In particular, although in both cases we have the scalings (32) the correlation functions obtained in the quasi-linear regime are not

given by a tree-model as in (100). This leads to the difference between the two-variable system (77)-(80) and the integral relation (117)-(118). Nevertheless, a simple prescription would be to recast the relations (117)-(118) into the form (77)-(80) by approximating the integrals over ϑ by the difference between two mean values, corresponding to the inner and outer regions of the filter U_{BV} and characterized by two averages τ_1 and τ_2. Then, the shift from the quasi-linear to the highly non-linear regime would simply be described by a smooth interpolation of the generating function $\zeta(\tau)$, i.e. of the sole parameter κ. However, such a study is left for a future work as in this article we preferred to lay out the formalism needed to study the statistics of the aperture mass and to focus on the two regimes which have already been tested in details against numerical simulations, so as not to introduce a new specific parameterization.

7. Conclusion

In this article we have described methods that allow exact reconstructions of the one-point PDF of the local aperture mass in weak lensing maps. These methods do take into account the projection effects but not all the nonlinear couplings between the local density field and the observed distortions field such as lens-lens coupling effects, or departure from the Born approximation.

In the course of this paper we have examined both the quasi-linear and non-linear regimes. In particular, although the details of the calculations are specific to each case we have pointed out the generic properties which are common to both regimes and the features brought about by the projection effects. For instance, in both quasi-linear and non-linear domains the PDF $P(M_{\mathrm{ap}})$ should show two asymmetric exponential tails. Our methods are quite general and can be extended in a straightforward fashion to other statistics. In the quasi-linear regime our approach can be applied to any filter which is axisymmetric while in the non-linear regime there are no restrictions. In particular, in this latter case our results can be extended to multivariate statistics (which can be obtained from filters which consist of several disconnected parts).

We have briefly investigated the dependence of the PDF $P(M_{\mathrm{ap}})$ with the shape of the filter. Thus, we have checked that for filters with a large compensation radius we recover approximatly the shape of the PDF $P(\kappa)$ which is relevant for the top-hat filtered convergence.

Finally, we have checked that our predictions agree reasonably well with the results of available numerical simulations (although we have not included any noise effect at this level) at scale about 4' where the data should provide the largest signal to noise ratio (e.g. Jain & Seljak 1997). In particular, we recover the asymmetric shape of the PDF. Moreover, our approach provides a prediction for the full shape of the $P(M_{\mathrm{ap}})$ while earlier models were restricted to the positive tail of the PDF. We have also shown that the difference between the PDFs obtained for two cosmologies (τCDM and OCDM) is larger than the inaccuracy of our predictions (due to parameterization we need to introduce to describe the underlying 3D density field). This suggests that

our results could be used to estimate the cosmological parameters. Thus, in addition to the skewness which is traditionally used to this purpose one could take advantage of the expected shape of the PDF to build other statistics which would maximize the dependence on the seeked parameters. Such a study is left for further work.

Appendix A: order of the singularity of $\varphi_{\mathbf{proj.}}(y)$

As noticed in Valageas (2000a) the exponent $\omega_{s,c}$ of the singularity of $\varphi_{\mathrm{cyl.}}(y)$ (as defined in (95)) translates into the exponent $\omega_{s,p} = \omega_{s,c} - 1/2$ for the projected generating function $\varphi_{\mathrm{proj.}}(y)$. However, in the cases encountered in this article we have $\omega_{s,c} = -3/2$ for both the quasi-linear and highly non-linear regimes. Then $\omega_{s,p} = -2$ is an integer but the generating function $\varphi_{\mathrm{proj.}}(y)$ is still singular at the points $y_{s\pm}^{\mathrm{proj}}$ through logarithmic factors. To see this, it is convenient to take the third derivative of the relation (34) which is governed by the singularity at $y_{s\pm}^{\mathrm{proj}}$ and diverges for $y \rightarrow y_{s\pm}^{\mathrm{proj}}$ (while the lower derivatives of $\varphi_{\mathrm{proj.}}(y)$ remain finite at $y_{s\pm}^{\mathrm{proj}}$). This yields:

$$\varphi_{\mathrm{proj.}}^{(3)}(y) = \int \mathrm{d}\mathcal{R}\, F(\mathcal{R})^3\, \psi_\theta(\mathcal{R})^2\, \varphi_{\mathrm{cyl.}}^{(3)}[y\, F(\mathcal{R})\psi_\theta(\mathcal{R})]. \quad \text{(A.1)}$$

For $y \rightarrow y_{s\pm}^{\mathrm{proj}}$ the integral is dominated by the values of $\mathcal{R}$ around the point where the factor $F(\mathcal{R})\psi_\theta(\mathcal{R})$ is maximum, since $\varphi_{\mathrm{cyl.}}^{(3)}$ diverges as $|y - y_{s\pm}^{\mathrm{proj}}|^{-3/2}$ at this point. Thus, we obtain from (A.1):

$$y \rightarrow y_{s\pm}^{\mathrm{proj}}: \ \varphi_{\mathrm{proj.}}^{(3)}(y) \sim \int_{-\infty}^{\infty} \mathrm{d}\mathcal{R}\, \left|(1-\mathcal{R}^2)y - y_{s\pm}^{\mathrm{proj}}\right|^{-3/2}. \text{(A.2)}$$

After the change of variable $t = |y/(y - y_{s\pm}^{\mathrm{proj}})|\mathcal{R}^2$ we obtain:

$$y \rightarrow y_{s\pm}^{\mathrm{proj}}: \ \varphi_{\mathrm{proj.}}^{(3)}(y) \sim \int_0^{\infty} \frac{\mathrm{d}t}{\sqrt{t}}\, (1+t)^{-3/2}\, \frac{|y|^{-1/2}}{|y - y_{s\pm}^{\mathrm{proj}}|} \quad \text{(A.3)}$$

which gives:

$$y \rightarrow y_{s\pm}^{\mathrm{proj}}: \ \varphi_{\mathrm{proj.}}^{(3)}(y) \sim \frac{1}{|y - y_{s\pm}^{\mathrm{proj}}|}. \quad \text{(A.4)}$$

Finally, the integration of this relation leads to:

$$y \rightarrow y_{s\pm}^{\mathrm{proj}}: \ \varphi_{\mathrm{proj.}}(y) \sim (y - y_{s\pm}^{\mathrm{proj}})^2\, \ln|y - y_{s\pm}^{\mathrm{proj}}| \quad \text{(A.5)}$$

where we only wrote the most singular term.

References

Bacon D., Refregier A., Ellis R., 2000, astro-ph/0003008
Balian R., Schaeffer R., 1989, A&A 220, 1
Bardeen J.M., Bond J.R., Kaiser N., Szalay A.S., 1986, ApJ 304, 15
Bernardeau F., 1994, A&A 427, 51
Bernardeau F., 1995, A&A 301, 309
Bernardeau F., Schaeffer R., 1992, A&A 225, 1
Bernardeau F., van Waerbeke L., Mellier Y., 1997, A&A 322, 1
Bernardeau F., Schaeffer R., 1999, A&A 349, 697
Bernardeau F., 1992, ApJ 392, 1
Blandford R.D., Saust A.B., Brainerd T.G., Villumsen J.V., 1991, MN-RAS 251, 600
Bouchet F.R., Schaeffer R., Davis M., 1991, ApJ 383, 19
Colombi S., Bernardeau F., Bouchet F.R., Hernquist L., 1997, MNRAS 287, 241
Groth E., Peebles P.J.E., 1977, ApJ 217, 385
Hui L., 1999, ApJ 519, L9
Jain B., Seljak U., 1997, ApJ 484, 560
Jain B., Seljak U., White S.D.M., 2000, ApJ 530, 547
Jannik G., Des Cloiseaux J., 1987, Les polymeres en solution, Les editions de physique, Les Ulis, France
Kaiser N., 1992, ApJ 388, 272
Kaiser N., 1998, ApJ 498, 26
Kaiser N., Wilson G., Luppino G.A., 2000, astro-ph/0003338
Kaiser N., Squires G., Fahlman G., Woods D., 1994, In: Durret F., Mazure A., Tran Thanh Van J. (eds.) Clusters of galaxies. Editions Frontières
Kruse G., Schneider P., 1999, submitted to MNRAS, astro-ph 9904192
Miralda-Escudé J., 1991, ApJ 380, 1
Munshi D., Bernardeau F., Melott A.L., Schaeffer R., 1999, MNRAS 303, 433
Munshi D., Coles P., Melott A.L., 1999, MNRAS 307, 387
Munshi D., Coles P., 2000, MNRAS 313, 148
Munshi D., Jain B., 1999a, astro-ph/9911502
Munshi D., Jain B., 1999b, astro-ph/9912330
Peacock J.A., Dodds S.J., 1996, MNRAS 280, L19
Peebles P.J.E., 1980, The large scale structure of the universe. Princeton University Press
Reblinsky K., Kruse G., Jain B., Schneider P., 1999, A&A 351, 815
Schaeffer R., 1984, A&A 134, L5
Schneider P., 1996, MNRAS 283, 837
Schneider P., van Waerbeke L., Jain B., Guido K., 1998, MNRAS 296, 873
Scoccimarro R., Frieman J.A., 1999, ApJ 520, 35
Tóth G., Hollósi J., Szalay A.S., 1989, ApJ 344, 75
Valageas P., 1999, A&A 347, 757
Valageas P., 2000a, A&A 354, 767
Valageas P., 2000b, A&A 356, 771
Valageas P., 2000c, submitted to A&A
Valageas P., Lacey C., Schaeffer R., 2000, MNRAS 311, 234
van Waerbeke L., et al., 2000a, astro-ph/0002500, accepted by A&A
van Waerbeke L., et al., 2000b, astro-ph/0009426, submitted to MN-RAS
Wittman D.N., Tyson J.A., Kirkman D., Dell'Antonio I., Bernstein G., 2000, astro-ph/0003014, to appear in Nature